JOURNAL OF GEOPHYSICAL RESEARCH, VOL. 89, NO. C4, PAGES 6533–6542, JULY 20, 1984

The Variation of Sea Surface Temperature in 1976 and 1977 2. The Simulation With Mixed Layer Models

K. MIYAKODA AND A. ROSATI

Geophysical Fluid Dynamics Laboratory/National Oceanic and Atmospheric Administration Princeton University

In connection with a study of the extreme weather events over the North American continent in January, 1977, analyses were performed to investigate characteristic properties of spatial and temporal variation of sea surface temperature for the years of 1976 and 1977, using world distribution of sea surface temperature described in the accompanying paper, part 1. The time evolution of ocean temperature patterns for these years are displayed by latitudinal distribution diagrams of sea surface temperature, and longitude-time (Hovmöller) diagrams. Gill-Turner's integral model and Mellor-Durbin's turbulence closure model of the mixed layer were applied to calculate the sea surface temperature anomaly in the northern hemisphere, using realisitic atmospheric forcing. Increase of time variability of the external forcing leads to an appreciably improved simulation of the sea surface temperature anomaly fields. Both models gave reasonable predictions for about 5 months in winter time, if the realistic external forcings were specified.

1. INTRODUCTION

It is perhaps the current understanding that the air-to-sea influence is direct and in situ, whereas the sea-to-air influence is complex and often of a teleconnection nature, except within the tropics. This teleconnection process has been pointed out in various ways by a number of authors. For example, the tropics-midlatitude connection was mentioned by *Bjerknes* [1966], the connection between the North Pacific and North America was mentioned by *Namias and Born* [1972], and the lag association between the North Atlantic sea temperature near Newfoundland and atmospheric pressure at the British Isles was mentioned by *Ratcliffe and Murray* [1970].

The impact of the sea surface temperature (SST) may be represented by an integral effect from various regions of the ocean. In particular, anomalous behavior of the SST over large regions has been connected with abnormal atmospheric development, and, concurrently, unusual weather phenomena. For this reason, to study a large-scale weather phenomenon over the United States it may be useful to know the SST not only over the North Pacific but over the Equatorial Pacific and even over the Atlantic Ocean.

Given the SST anomaly analysis as described by *Miyakoda and Rosati* [1982], the large-scale SST temporal and spatial variation, during 1976 and 1977 will be examined. Some details of the SST structure will be discussed in relation to readily observable phenomena. Possible explanations for the development and evolution of particular SST anomaly patterns will be suggested by means of comparative studies using two different types of ocean mixed layer models. As a sidelight, a comparison of the two types of models suggests further information concerning the SST evolution during 1976 and 1977.

The years 1976 and 1977, for which extensive oceanic and atmospheric data were available, were characterized by relatively rapid development of localized anomaly extrema, interspersed with relatively persistent anomaly patterns. Concomitantly, extreme weather patterns were experienced over North America, which makes investigation of these years particularly appropriate. Some possible causes of small-scale anomaly variability will be suggested. Other authors, such as *Haney* [1980] and *Denman and Miyake* [1973], have investigated ocean behavior in small regions or at selected ocean stations. In this study, some explanations for SST anomaly behavior over larger areas of the northern hemisphere will be attempted, since these regions may be important for understanding the abnormal atmospheric events.

Paper number 4C0458.

2. LATITUDINAL DISTRIBUTION

In general, the 1976 and 1977 SST's as produced by the analysis described in *Miyakoda and Rosati* [1982], exhibit changes in both latitudinal and longitudinal directions. To obtain insight into the north-south variability, zonal averages were taken for the SST analysis, for the Rand climatological SST [*Alexander and Mobley*, 1976], and for the climatological SST from *Levitus and Oort* [1977]. By using monthly means for the Pacific Ocean for each latitude, Figures 1*a* and 1*b* were produced. For comparison, an annual average of the zonal mean Rand values was subtracted from the above mentioned quantities.

One can observe in Figures 1*a* and 1*b* that the magnitudes of the anomalous SST for the Pacific Ocean are of the order of ± 3°C. The two climatologies are generally the same, i.e., no systematic bias was detected. Nevertheless, it is interesting to note that differences between the two climatologies in some instances are as large or larger than the difference between the SST analysis and a climatology (see the recent article by *Reynolds* [1983]). This illustrates the delicate nature of SST anomaly prediction. The persistence of the SST anomaly patterns is noted, with gradual changes from one month to the next. Notable features are negative anomalies at 0°–20°N from January to May of 1976 and 1977 and negative anomalies at 50°–60°N from July to October of 1976 and 1977. A consistent feature during all months is a warm anomaly between 20°–40°S and a cold anomaly farther south.

A possible pattern recurrence is indicated in the winter months of both years in the North Pacific anomaly component. *Namias and Born* [1970, 1974] ascribed the pattern recurrence to storage of anomalously cold or warm water that is shielded by a shallow layer in summer but is stirred up to the

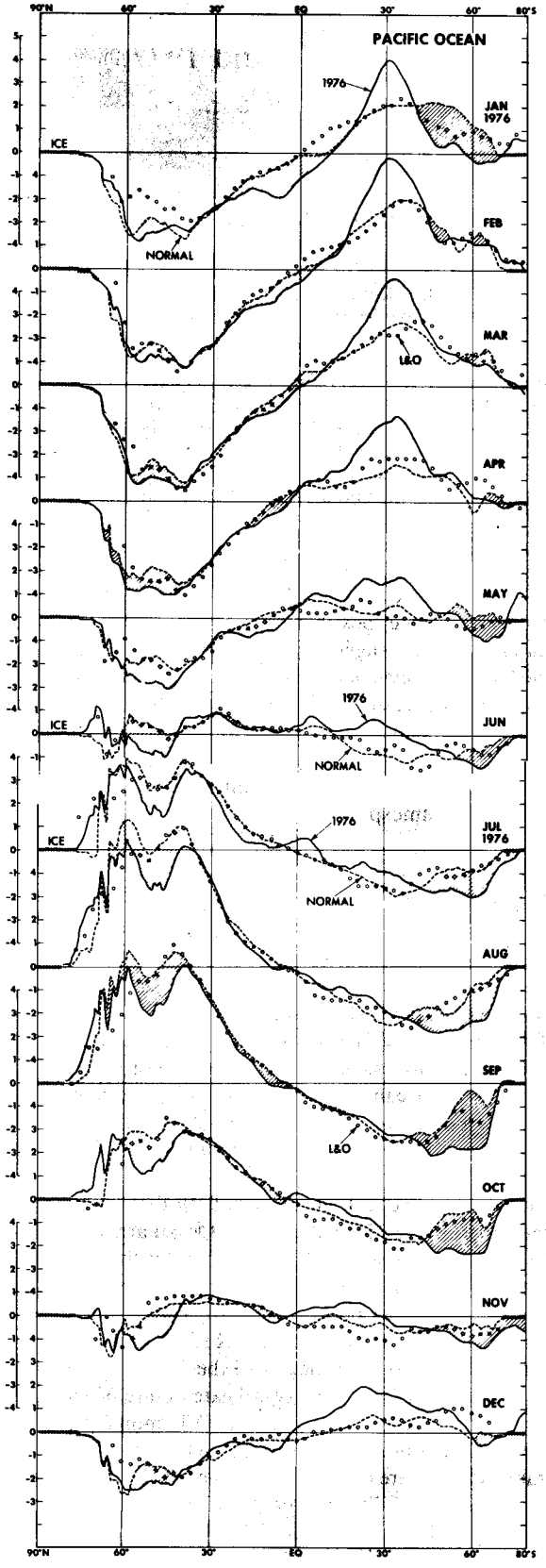

Fig. 1*a*. Monthly variation of SST in 1976 over the Pacific Ocean. All the curves and circles indicate departures (°C) from the climatological annual mean of SST at the respective latitude. The solid lines are 1976 values obtained from the amalgamated analysis of ship and satellite data. The dashed lines are the RAND climatological normals and the normals of Levitus and Oort are shown by small circles. Negative anomalies area are shaded.

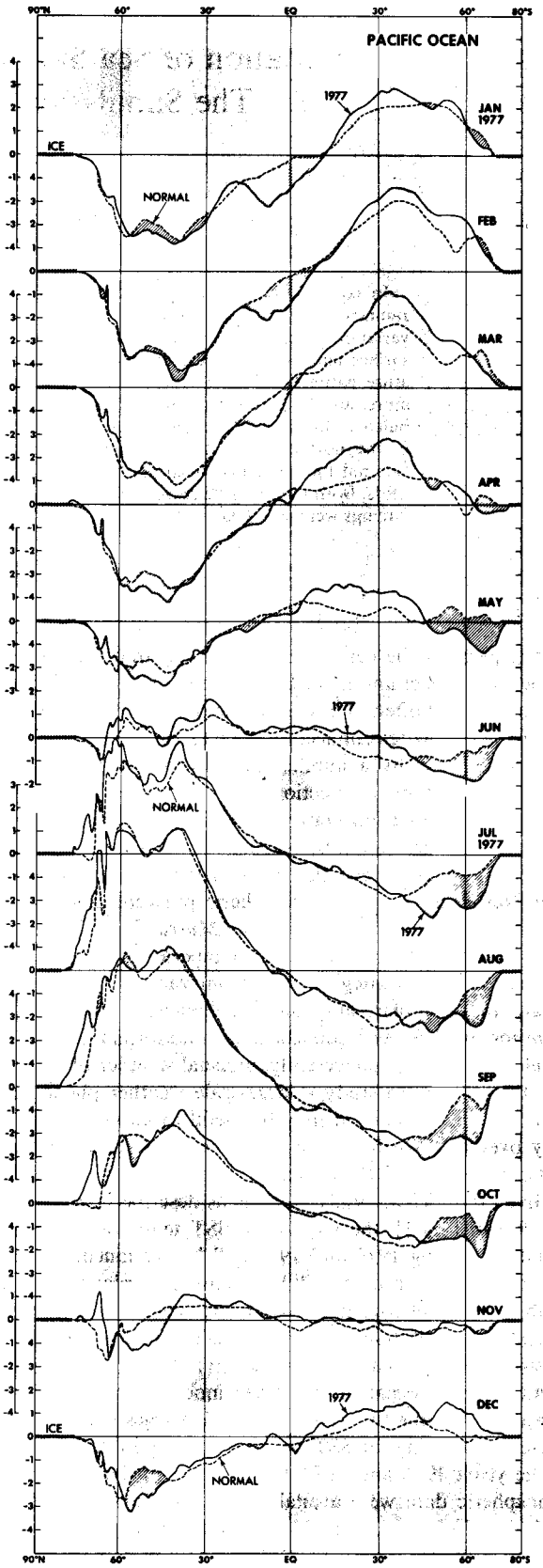

Fig. 1*b*. The same as in Figure 1*a* but for 1977.

surface by the increased wind stress during cold months. This possible recurrence feature, especially indicated in January through March of 1976 and 1977, may be present in the anomalies as well as in the seasonal cycle. Other similarities

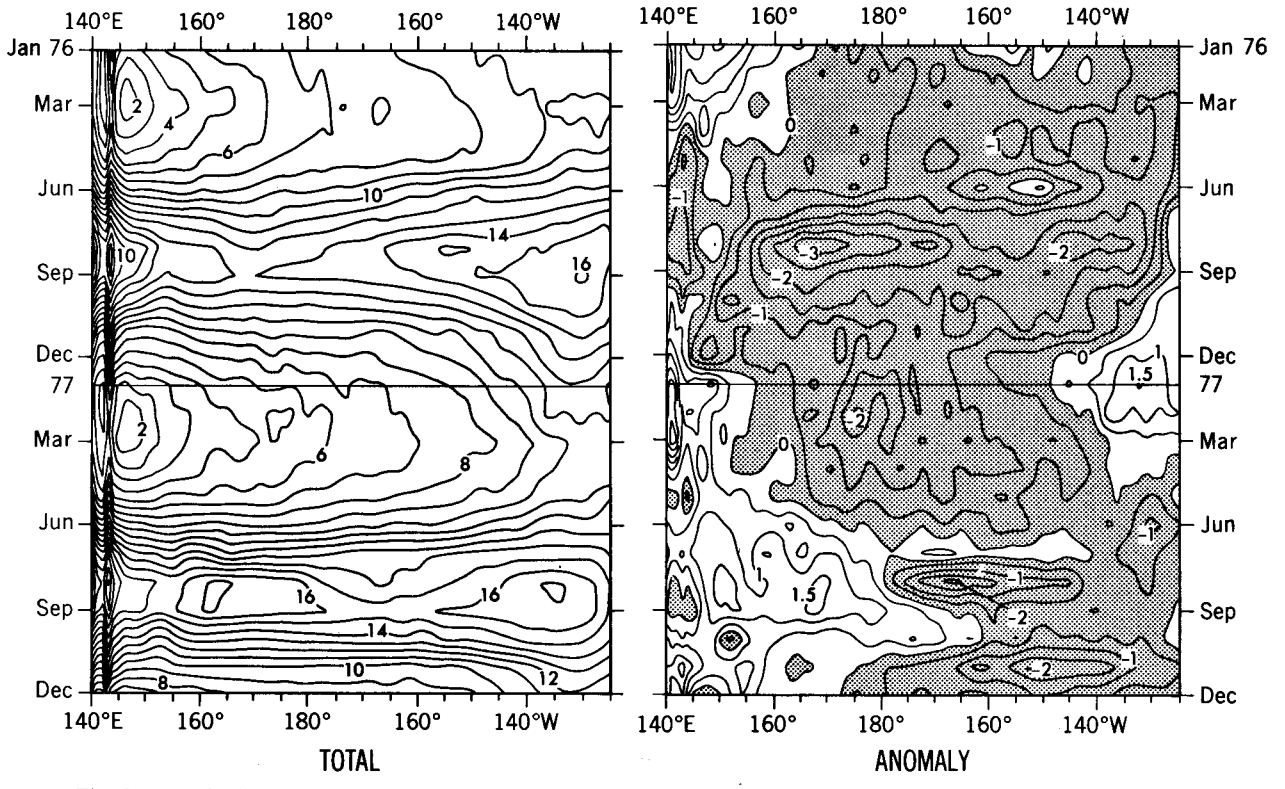

Fig. 2. Longitude-time chart of SST (°C) total (left) and anomalies (right) for 40°–50°N belt in the North Pacific. The ordinate is time, directed downward from January 1976 to December 1977. Negative values are shaded.

from year to year could reveal similarities in seasonal atmospheric forcing patterns on interannual time scales. This may be particularly true on the regions of the subtropical and subarctic oceanic gyres. Evidence for such coherence of SST anomalies was given by *Middleton* [1980].

The point to be emphasized here is the capricious nature of SST anomalies, and the delicate task of predicting them on a large scale. While the seasonal cycle of SST may be reproduced with fair accuracy, a different degree of difficulty resides in predicting anomalies, which are relatively small compared to the total field.

3. Hovmöller Diagrams

Another way of looking at temporal and spatial variation of SST anomalies over selected regions is by constructing a longitude-time chart, or Hovmöller diagram. In this manner, differences across a latitude line may be quantified, as well as measured against Rand climatology. The region between 40° and 50°N of the North Pacific is of considerable interest in connection with the extraordinary weather event of January 1977.

Figure 2 is a diagram of the SST and corresponding anomalies for the North Pacific (40°–50°N) where the latitudes in parenthesis indicate the domain of the average. In these diagrams the monthly mean SST values are based on the amalgamated analysis of ship-of-opportunity reports and of satellite soundings as described in part 1.

One may note a similar type of SST structure across the zone in the North Pacific (Figure 2) up to June 1977, with localized intense negative anomalies interspersed. The general character of this pattern over 18 months may reflect consistent atmospheric forcing patterns associated with flow along the subarctic gyre, as indicated by *Middleton* [1980]. *Ciesielski* [1980] found maxima of mean wind speed and wind speed variance where the intense negative SST anomalies are located in Figure 2, possibly indicating a cause-effect relationship. A maximum in cyclonic activity also reported by *Petterssen* [1956] seems to coincide with the centers of largest anomalies. The detailed structure near the western boundary of Figure 2 could represent meanders in the Kuroshio-Oyashio confluence zone. A positive anomaly persisted from October 1976 to March 1977, which corresponds to the warm water observed off the west coast of the United States during this period. Little large-scale movement seems to be observed in the Pacific SST anomaly, again reinforcing the suggestion by *Ciesielski* [1980] that in mid-oceanic regions in situ surface processes, rather than advection, etc., account for observed SST anomalies. In sections 5 and 6, the results of the simulation with mixed layer models, we will attempt to evaluate this point.

In summary, inspection of SST's on a large scale in 1976 and 1977 seems to reveal the suggested importance of surface processes and atmospheric forcing in large portions of the ocean basins.

4. Mixed Layer Models Used for Simulation

To gain some insight into the causes of the SST anomaly patterns during 1976 and 1977, an attempt was made to simulate anomaly patterns using observed atmospheric forcing. Evaluation of model performance could yield information concerning the importance of surface mixing/heating versus other possible causes in defining the large-scale SST behavior.

There are in general two classes of the mixed-layer models, i.e., "the integral model" and "the multilevel model." The first class includes *Kraus and Turner* [1967], *Kitaigorodosky and Miropolsky* [1970], *Pollard et al.* [1973], *Denman* [1973], *Denman and Miyakde* [1973], *Niiler* [1975], and *De Szoeke and Rhines* [1976]. The second class includes *Mellor and Durbin* [1975], *Marchuk et al.* [1977], *Madsen* [1977], and

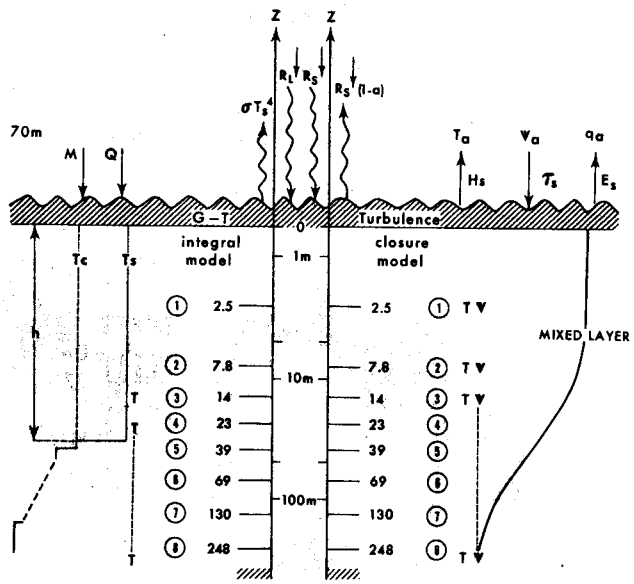

Fig. 3. Schematic illustration of the vertical levels and the atmospheric forcings for the Gill-Turner model (left) and the turbulence closure model (right).

Kondo et al. [1979]. The two specific models applied in this paper are the *Gill and Turner* [1976] model and the *Mellor and Durbin* [1975] model. These mixed-layer models differ in their prescription of surface mixing processes occurring in conjunction with the atmospheric forcing.

4.1. *Gill-Turner Model*

This model is based on the original work of *Kraus and Turner* [1967] and falls into the class termed "integral theories." By considering the layer to be homogeneous and eliminating eddy diffusivities, relatively easy solutions based on energy balance considerations are found. The existence of a mixed layer is assumed a priori, rather than a consequence of available oceanic boundary conditions.

The Gill-Turner model includes equations for the heat content H and for potential energy P,

$$H = \int_D^0 T\, dz \tag{1}$$

$$P = \int_D^0 ZT\, dz \tag{2}$$

where T is temperature, Z is depth, and D is the bottom depth of the model. The model is based on the principle that mechanical turbulence generated by the surface wind changes the potential energy of the temperature profile by mixing buoyant water downward from the surface.

4.1.1. *Basic equations.* Denoting the surface input of heat by Q, and the surface input of mechanical energy due to wind mixing by M (see Figure 3), the equations of the Gill-Turner model may be written as

for $Q \geq 0$ (heating)

$$dH/dt = Q \tag{3}$$

$$dP/dt = M + \tilde{S} \tag{4}$$

and for $Q < 0$ (cooling)

$$dH/dt = Q \tag{5}$$

$$dP/dt = \tfrac{1}{2}h(1-\mu)\, dH/dt + M + \tilde{S} \tag{6}$$

where $\tilde{S}$ is the solar heat flux through the surface; μ is an entrainment parameter due to penetrative convection at the base of the mixed layer.

4.1.2. *External forcing.* The formulation for the rate of mechanical stirring M is based on the laboratory experiments of *Kato and Phillips* [1969] as

$$M = 1.25/[g \cdot \alpha(T)]U_*^3 \tag{7}$$

where $U_* = (\tau_w/\rho_w)^{1/2}$ is the ocean friction velocity, g is gravity, and $\alpha(T)$ is the coefficient of thermal expansion. In this case, ρ_w is the ocean density and τ_w is the surface ocean stress, assumed equal to the atmospheric stress τ_a at the interface. From equations (3)–(6), the mixed layer temperature T_s and depth h may be derived.

Surface boundary conditions for the Gill-Turner model may be determined by a heating term and a momentum flux term. Heat flux Q at the interface is given by

$$Q = [R_s\downarrow(1-a) + R_L - \varepsilon\sigma T_s^4 - H_s - LE_s] \tag{8}$$

where $R_s\downarrow$ is the portion of insolation absorbed near the surface, a is the albedo, $R_L\downarrow$ is the downward longwave flux. R_s, a, and $R_L\downarrow$ are produced as climatologies from a grid point atmospheric model assuming a zonal distribution of cloudiness. The term $\varepsilon\sigma T_s^4$ is a longwave upward flux term, where σ is the Stefan-Boltzman constant, and ε is the emissivity. L is the latent heat. Sensible heat flux H_s is given by

$$H_s = \rho_a C_p C_H |W_a|(T_s - T_a) \tag{9}$$

where ρ_a is the air density and C_p is the specific heat at constant pressure, C_H is the bulk aerodynamic exchange coefficient, $|W_a|$ is the wind magnitude at 70 m above the ocean surface, and T_a is the air temperature also at 70 m. Values of $|W_a|$ and T_a were obtained twice a day from a NMC level III Hough analysis (NMC, National Meteorological Center, Washington, D. C.) of observed winds and temperatures for the northern hemisphere for 1976 and 1977. Similarly, the evaporative flux E_s is given as a bulk aerodynamic expression as

$$E_s = \rho_a C_E |W_a|(q_s(T_s) - q_a) \tag{10}$$

where C_E is an evaporative exchange coefficient, $q_s(T_s)$ is the saturation mixing ratio at the ocean surface for T_s, and q_a is the atmospheric mixing ratio, which was taken to be the monthly mean climatology of *Oort* [1977].

The momentum boundary condition is given by a wind stress, τ_a, defined as

$$\tau_a = \rho_a C_D |W_a|^2 \tag{11}$$

where C_D is the drag coefficient and, again, $|W_a|$ is taken from observed wind measurements. Use of this type of bulk aerodynamics method was indicated by *Esbensen and Reynolds* [1981].

Values of C_H and C_E were held constant at 1.1×10^{-3}, and C_D was set to 1.5×10^{-3}. These values lie in the middle range of values as determined by *Bunker* [1976] from experimental data.

4.1.3. *Boundary conditions.* A bottom boundary condition for this one-dimensional model is that heat flow is zero, i.e., no heat is allowed to escape.

4.1.4. *Levels and grids.* Figure 3 illustrates schematically, on the left, the form the temperature profile of the upper layers of the ocean is assumed to have. The number of levels is eight extending from the surface to a depth of 248 m. It is assumed that a surface mixed layer exists with a temperature T_s, and a

discontinuity in temperature T_c, at the base of the mixed layer. The depth h is carried as an extra variable so that changes in the mixed layer depth are not restricted by the vertical resolution of the model.

The horizontal domain covers the Northern Hemisphere. The grid [*Bryan and Lewis*, 1979] is a latitude-longitude grid. The east-west grid spacing is 5.6°, and the north-south grid spacing is 4.5°.

4.2. *Mellor-Durbin Model*

The second class of mixed layer models is based on the turbulence closure method. In this approach, the vertical profiles of the turbulent variables are obtained as a solution of a closure system of turbulence and thermodynamic equations. Thus the vertical structure within the upper layers, which need not be well mixed, can be predicted in more detail by this method than by the former method. Only one-dimensional diffusive processes are considered here; advective, horizontal, etc., processes are neglected.

4.2.1. *Basic equations.* The model equations are

$$\frac{\partial u}{\partial t} = fv + \frac{\partial}{\partial z}\left[(\nu + K_M)\frac{\partial u}{\partial z}\right] \tag{12}$$

$$\frac{\partial v}{\partial t} = -fu + \frac{\partial}{\partial z}\left[(\nu + K_M)\frac{\partial v}{\partial z}\right] \tag{13}$$

$$\frac{\partial T}{\partial t} = \frac{\partial}{\partial z}\left[(\kappa + K_H)\frac{\partial T}{\partial z}\right] \tag{14}$$

where f is the Coriolis parameter, K_M is the eddy viscosity, K_H is thermal diffusivity, and ν and κ are molecular viscosity, and conductivities of heat, set at 1 cm^2 s^{-1} and 0.1 cm^2 s^{-1}, respectively.

Values of K_M and K_H are obtained by a turbulence closure model presented by *Mellor and Durbin* [1975] and are given by

$$K_H = lbS_H \tag{15}$$

$$K_M = lbS_M \tag{16}$$

where b is the square root of twice the turbulent kinetic energy, l is a turbulence length scale, and S_M and S_H are flux Richardson number R_i dependent stability factors [*Mellor and Yamada*, 1974], where

$$R_i \equiv \beta \cdot g \frac{\partial T}{\partial z} \Big/ \left[\left(\frac{\partial u}{\partial z}\right)^2 + \left(\frac{\partial v}{\partial z}\right)^2\right] \tag{17}$$

Here, g is the acceleration of gravity and β is the coefficient of thermal expansion. S_M and S_H are determined in such a way that turbulence disapppears at $R_i = 0.23$. Given newly computed values of K_M and K_H, values of u, v, T are computed at every time step.

The quantity b is calculated from a form of the turbulent kinetic energy equation representing a balance between shear production, buoyancy production and dissipation:

$$lbS_M\left[\left(\frac{\partial u}{\partial z}\right)^2 + \left(\frac{\partial v}{\partial z}\right)^2\right] - lbS_H\left(\beta g \frac{\partial T}{\partial z}\right) - \frac{b^3}{15l} = 0 \tag{18}$$

Following *Mellor and Durbin* [1975] we calculate the turbulence length scale from the ratio of the first to the zero-th moment of the turbulence field:

$$l = \alpha_1 \int_{-\infty}^{0} |z|\, b\, dz \Big/ \int_{-\infty}^{0} b\, dz \tag{19}$$

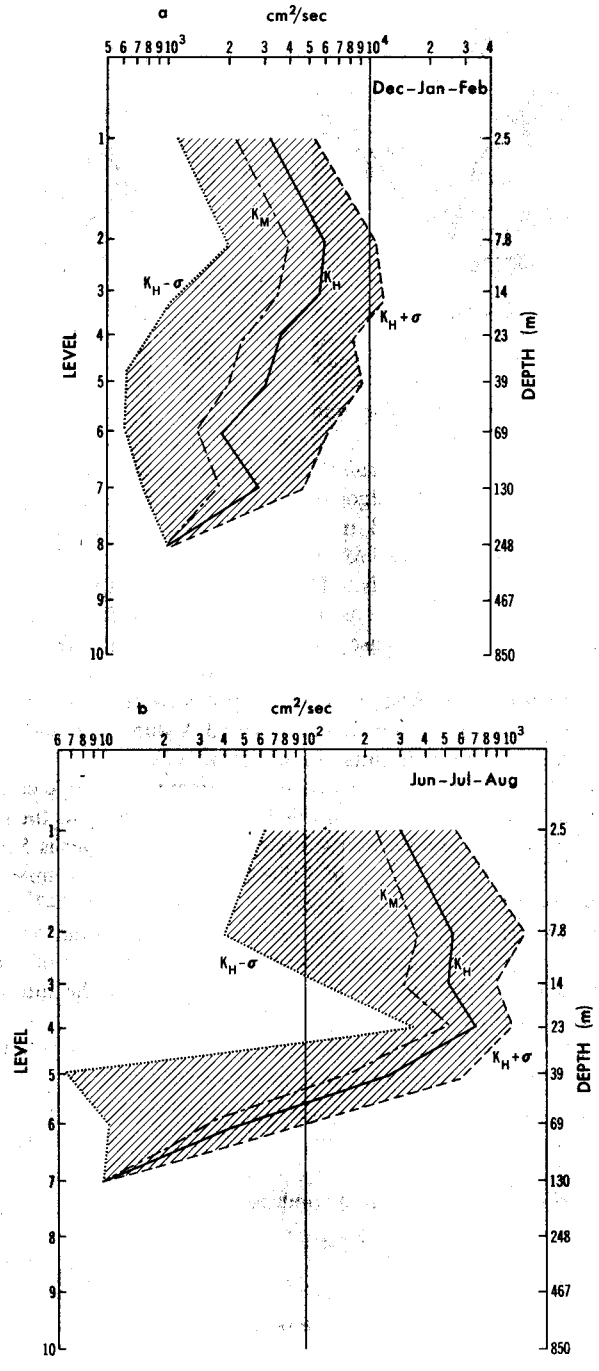

Fig. 4. An example of vertical distribution of turbulent eddy coefficients, K_M and K_H, at a point of 42.75°N and 172°W for two different seasons. The range between $K_H + \sigma$ and $K_H - \sigma$ is shaded, where σ is the standard deviation.

where $\alpha_1 = 0.20$. This equation, plus (15)–(18), closes the turbulence parameterization.

Perhaps it is necessary to mention that this approach uses empirical constants, determined by laboratory experiments, for the subgrid scale parameters, and they can be applied as universal constants to the ocean as well as to the atmosphere.

Figure 4 indicates the vertical distributions of K_M and K_H at 47°N, 172°W for the warm and cold seasons. The K_M values are generally smaller than for K_H. This is also the case for the atmosphere [see *Miyakoda and Sirutis*, 1977]. In the warm season, K_M and K_H are small because the thermal stratification tends to be stable and the wind stress is weak; and in the cold season, K_M and K_H become very large.

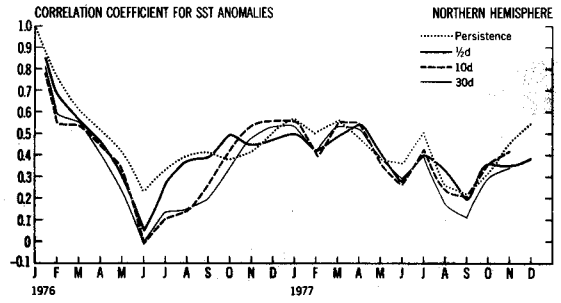

Fig. 5. Correlation coefficients of the SST anomalies between the simulation and the observation over the northern hemisphere for the cases of 30-day, 10-day mean and half day atmospheric forcings.

4.2.2. *Radiation.* The same treatment as in the Gill-Turner model is used.

4.2.3. *Numerical calculation.* Diffusion equations were solved with an implicit algorithm, where the z integration proceeds with the standard tridiagonal matrix reduction technique [see *Richtmyer and Morton*, 1967].

4.2.4. *Levels and grids.* The horizontal grid spacing and type of grid are the same as previously discussed for the Gill-Turner model. In this case there are eight vertical levels (see Figure 3) down to 248 m, with increased resolution near the surface, where the first level is 2.5 m below the surface as shown on the right-hand side of Figure 3. Values of T and W are located at the midpoints of each layer.

Kondo et al. [1979] discussed the treatment of oceanic constant flux layer. The depth of this layer is, according to them, about 63 cm, whereas in our study the uppermost layer is 5 m deep. *Elsberry and Garwood* [1980] mentioned that mixed layer models typically use vertical increments of 1–3 m, whereas the oceanic GCM (general circulation model) may have layers 10–100 m thick. In our case, the decision of the vertical resolution was made in conjunction with the future use of a GCM [*Philander and Pacanowski*, 1981].

4.2.5. *Boundary conditions.* The heat flux boundary condition is the same as in the Gill-Turner model, i.e.,

$$\rho c_p K_H \left.\frac{\partial T}{\partial z}\right|_{z=0} = Q \tag{20}$$

Similarly, for the momentum condition,

$$\rho K_M \left.\frac{\partial W}{\partial z}\right|_{z=0} = \tau_a \tag{21}$$

The boundary conditions for the bottom are

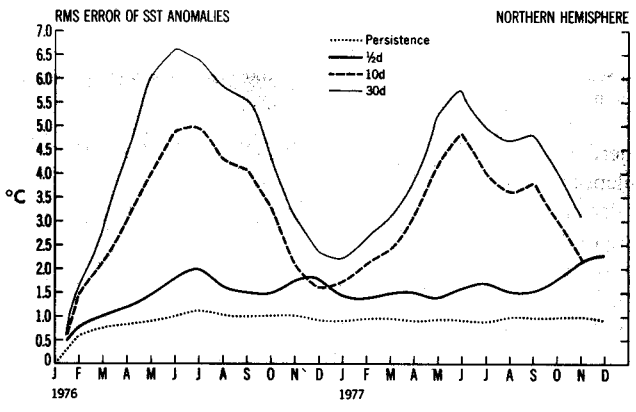

Fig. 6. Root-mean-square difference of the SST between the simulation and the observation over the northern hemisphere for the cases of 30-day 10-day mean and half day atmospheric forcings.

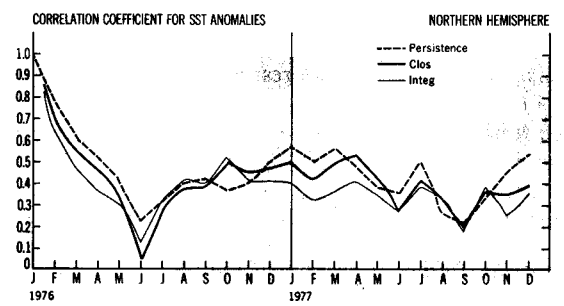

Fig. 7. Correlation coefficients of the SST anomalies between the simulation and the observation over the northern hemisphere for the case of 1976 and 1977 with the closure model. The result of the integral model with twice daily atmospheric forcing is also shown for reference.

$$\frac{\partial}{\partial z}(u, v) = 0 \tag{22}$$

$$\frac{\partial T}{\partial z} = 0 \tag{23}$$

Simulations using these two types of one-dimensional mixed layer models will be made to attempt to predict SST anomaly patterns.

5. Results of the Simulations

The initial temperature profiles, for both models, were obtained by using the observed SST at the first layer and extending it down to the nearest layer corresponding to the climatological mixed layer depth, as given by *Levitus* [1982]. Climatological values [*Levitus*, 1982] are used to initialize temperature below the mixed layer. This initialization procedure is one method of estimating subsurface temperatures when observations over the entire domain are not readily available.

Given initial conditions in mid-January 1976, obtained from the initialization procedure previously described, simulation runs were performed using the turbulence closure model. The geographical distributions of SST for 1976 and 1977 were obtained for various atmospheric forcings, i.e., the monthly mean, the 10-day mean, and the half day forcing for V_a and T_a. The SST anomaly patterns were verified against the observed anomalies [*Miyakoda and Rosati*, 1982].

Figures 5 and 6 show correlation coefficients and rms errors for the turbulence closure simulation. Points considered to

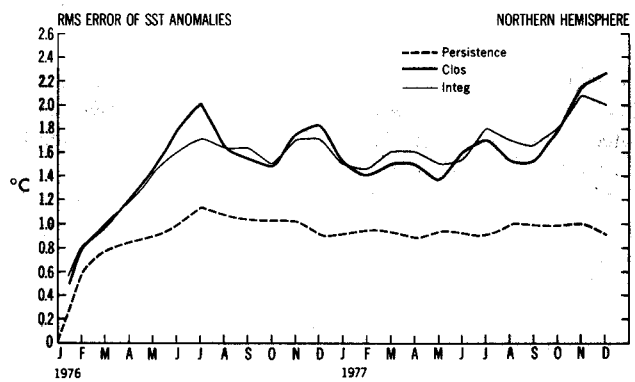

Fig. 8. Root-mean-square difference of the SST between the simulation and the observation over the northern hemisphere for the case of 1976 and 1977 with the closure model. The result of the integral model with twice daily atmospheric forcing is also shown for comparison.

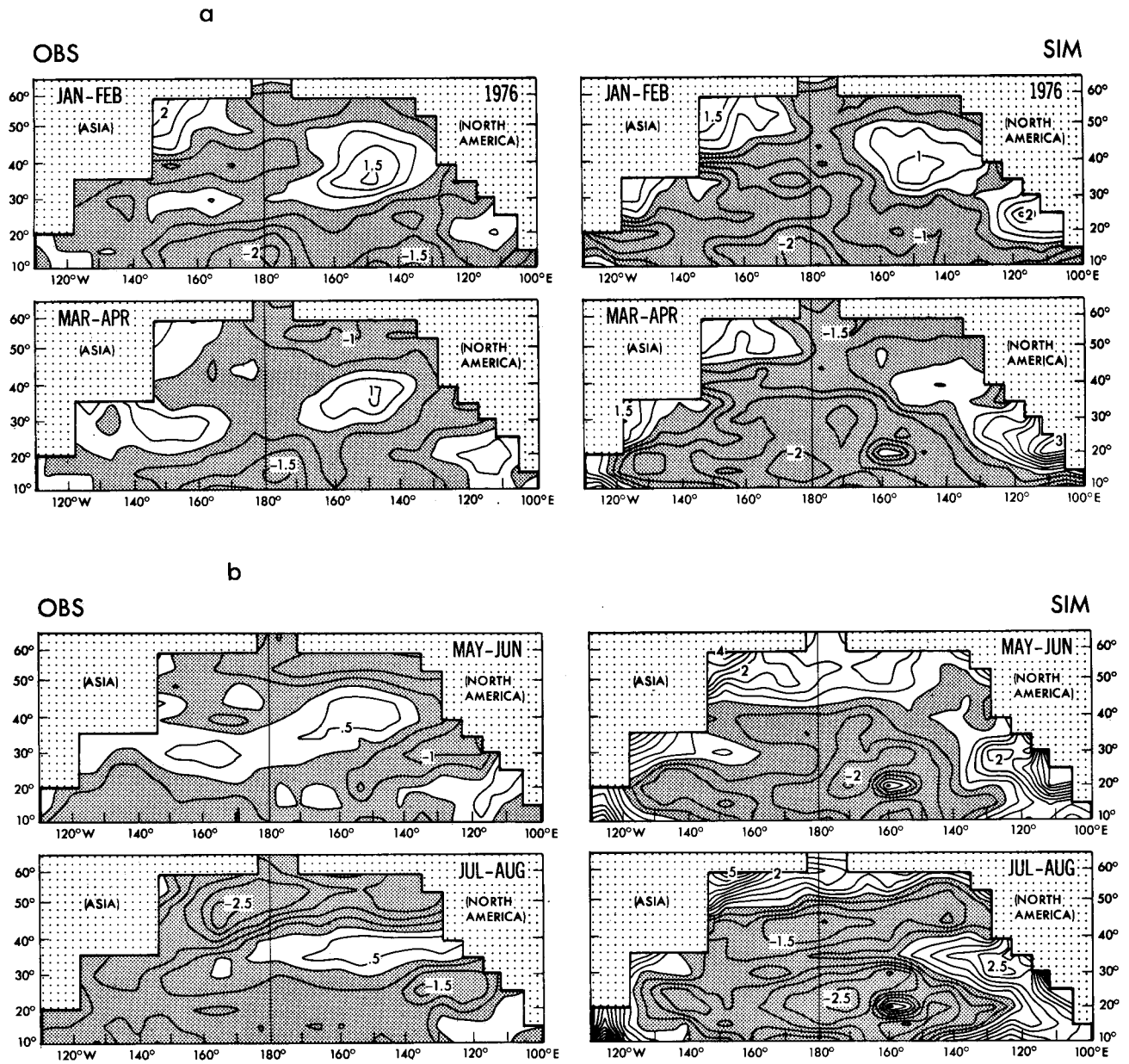

Fig. 9. (*a*) Comparison of the simulations (sim) and observations (obs) of SST anomalies over the north Pacific for January–April 1976. Units are °C and the contour interval is 0.5°C. The negative areas are lightly shaded, and the areas in which the anomaly is less than −2.5°C are dark. (*b*) The same as in Figure 11 but for May–August 1976.

represent ice were eliminated. We see in Figure 5 that the correlation coefficients are not very different for the three cases, although the half day case is slightly better. However, Figue 6, the rms error, shows a systematic improvement during the heating season for the half day case over the 10- and 30-day cases. It is hypothesized that increased wind-stirring, associated with shorter time averaging, is responsible for a deeper mixed layer and lower SST's. This process appears to be most critical in regions of very shallow mixed layer, i.e., around subarctic gyres, and, less importantly, in the subtropical regions toward the equator, where the annual variation of mixed-layer depth is smaller. The wind stress computed from monthly mean winds is too weak, whereas the half day or the 10-day mean forcing includes the intermittent effects of storm passages, which serve to increase the vertical mixing and hence decrease the SST [*Halpern*, 1974]. In the winter, other processes are important in determining the SST, and the magnitude of the wind is generally larger, so that time-averaging is not as detrimental. For the same reasons, the differences in results with the half day case are even more graphic in Figure 6 than in Figure 5. It appears that Figures 5 and 6 reinforce the suggestion that surface wind-stirring played an important role in determining the SST anomalies in the summer of 1976. The maxima in correlation in the winter-time indicates that the "recurrence" effect mentioned by Namias and his colleagues is present not only in the normal component but also in the anomaly component of SST. This feature indicates the importance of specifying properly the thermocline temperature in the initial conditions.

A 2-year simulation was performed for 1976 and 1977 using both the turbulence closure and integral models with half day atmospheric forcing. Results of Figures 7 and 8 indicate that the simulation skill score is relatively high in the first 5–6 months and it decays rapidly, that the skill is even worse than

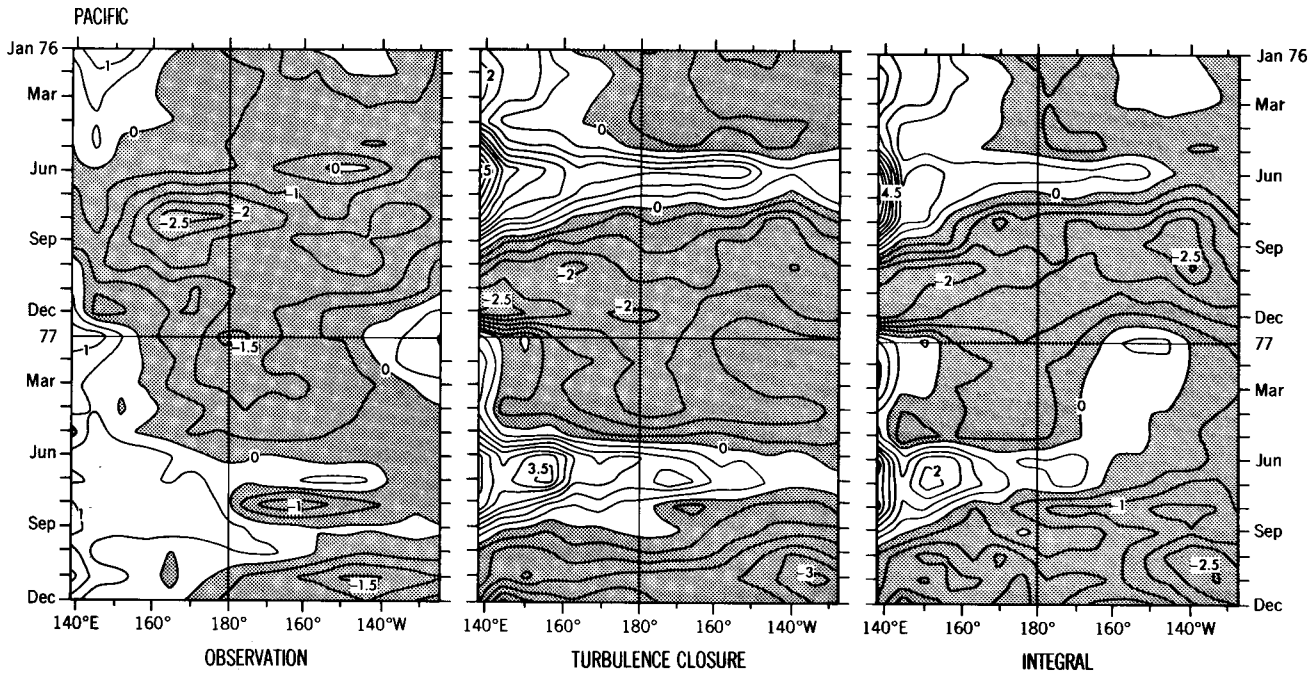

Fig. 10. Hövmoller diagrams of three anomaly fields of SST, averaged over 40°–50°N in the Pacific; the observed SST in °C (left) the simulation by the closure model (middle), and the simulation by the integral model (right). Negative areas are shaded.

persistence, and that both models give very similar results in terms of statistics. The rapid deterioration of the simulation appears to be due to excessive warming of seawater. More efficient mixing or lateral advection is needed. The performances of both models are similar. In other words, we are unable to determine a superiority of one model over another. It appears that the quality of data, particularly moisture and radiation, hindered a precise investigation of the performance.

In a pictorial manner, it is to be desired to infer the role of surface mixing in creating observed SST anomalies by looking at two-month averages of SST anomalies, both observed, and simulated (closure model), from an initial time of January 1976 (Figures 9*a*, 9*b*).

Tendencies of the anomaly developments during January through April 1976 on the Pacific seem to be well captured by the closure model. Even in the Kuroshio-Oyashio confluence zone, the reduction in size of the positive SST anomaly pattern is well represented. One should note that at this time of year, accurate thermocline specification is probably important, but changes in surface cooling rates could have a marked effect on the anomaly patterns. Persistence of the observed SST anomalies, as discussed previously, for the period of 1976 is pronounced over all regions of the Pacific, and this gradual change is reproduced, to some extent, by the model.

Model performance in simulating observed SST anomalies diminishes appreciably during May through August 1976. The simulations are too warm in the region of the subarctic gyre, although there are suggestions of a warm "tongue" protruding across the subtropical gyre in the simulation. The simulations are poor in the western boundary region, possibly due to anomalously strong advective processes occurring at this time. Although the cooling tendencies of the observations from May–June to July–August are essentially reproduced over the entire region by the model, the strength of the negative anomalies are underrepresented.

Figure 10 is the comparison of Hövmoller diagrams between the observation and the simulations by the turbulence closure model and the integral model. The cooling tendency in September–December and the warming tendency in May–July agree with each other in the simulation and the observation, and some observed features of SST variability are reproduced by the models. However, the extreme coldness in summer of 1976 is not well reproduced. Figure 9*b* suggests that this failure is due to excessive heating in the neighboring high latitudes. In general, the summer warmings are dominant in the simulation of both models, indicating that other effects have to be incorporated.

In summary, large-scale agreement between the models and observations of SST anomalies indicate that surface forcing may play a major role in large-scale development of SST anomalies, but the simulated SST's include excessive heatings in summer.

6. THE INTEGRAL VERSUS CLOSURE MODELS AND OTHER REMARKS

An advantage of the integral model method is the conceptually simple account of the mixed layer process, and if applied, the method is economical but possibly lacks accuracy. On the other hand, an advantage of the closure model method is the mathematically rigorous formulation of the turbulent variances and covariances. Although the method is quantitative, it is somewhat expensive. The computer times in our study were 0.25 min/year for the former method and 3 min/year for the latter method with the Control Data Corp. Cyber 205.

Differences in mixing characteristics between the two types of models near the surface in summer, as well as in the mixed layer deepening characteristics in winter are shown to have some importance in prescribing SST development. The general tendency shown is that a detailed thermal and velocity structure, as in the closure model, more closely approximates the relatively rapid SST anomaly development and transient be-

havior. More persistent observed anomaly behavior may be better simulated by the integral model. However, these results indicate that both models give quite similar results.

Results presented in this paper have some noticeable deficiencies such as the SST's in the higher latitudes and the eastern subtropics during the summer months are excessively warm and also the amplitude of the SST anomaly is too large. Some of the possible reasons for this are

1. This is a one-dimensional model and therefore lacking the horizontal and vertical processes of a three-dimensional model, which may be important as suggested by *Adem* [1970], *Daly* [1978], and *Haney et al.* [1978].
2. The vertical mixing in these areas is underestimated.
3. This model does not simulate ice and therefore during the heating season energy goes directly into heating the ocean and not into melting ice in the subarctic region.
4. Accurate and real-time observed insolation and/or mixing ratio, rather than climatology, could be necessary.
5. More accurate wind data could improve the vertical mixing.

In order to determine which of these processes is the most probable contributor to the poor simulation some experiments were run. By using the three-dimensional model of *Bryan and Lewis* [1979], with the closure model included on the same grid, and the same atmospheric forcing used in the one-dimensional models, simulations were run. Analyzing the difference maps of the three-dimensional to one-dimensional monthly means it did not appear that the tendency of the warm SST's was corrected. In fact, in the subarctic region it was even warmer. It does not appear, at least in the this preliminary study, that the gross deficiencies we see are due to the lack of the additional processes included in a three-dimensional model. The next experiment tried to ascertain the effects of increased vertical mixing. This was accomplished simply by increasing the background mixing in the closure model and rerunning. The results did show a cooling tendency and reduction in the excessive warming. This may indicate that if we were to use a higher-order closure scheme, where the mixing is better represented, the results could be improved. Tests with the atmospheric forcings will await other, perhaps more accurate, data sources.

7. CONCLUSIONS

There are five major conclusions.

1. The mixed layer model of the ocean used in this study was, to some extent, capable of simulating the SST anomaly fields in 1976 and 1977 for 4–5 months ahead in winter with some skill, using the real atmospheric forcings.
2. The turbulence closure model and the integral model produced similar simulations of the SST fields. However, the integral model requires much less computational resources.
3. Namias "recurrence" effect in the wintertime was noticed even in the anomaly component of SST. This may imply that the initial conditions of sea temperature for the seasonal thermocline are important for the winter prediction of SST.
4. When the atmospheric forcing is averaged in time the results indicate a significant difference in the amplitude of the error but not the phase. This does indicate without the proper time resolution for the atmospheric forcing the heat storage of the ocean could have quite a large error.
5. In order to improve the simulation performance, the external forcing data, such as the moisture in the atmosphere, the air temperature and the radiation should be of better quality; the turbulence closure model should be more advanced than that of the hierarchical level 2.0.

REFERENCES

Adem, J., On the prediction of mean monthly ocean temperatures, *Tellus, 22*, 410–430, 1970.

Alexander, R. C., and R. I. Mobley, Monthly average sea-surface temperature and ice-pack limits on a 1° global grid, *Mon. Weather Rev., 104*, 143–148, 1976.

Bjerknes, J., A possible response of the atmospheric Hadley circulation to the equatorial anomalies of ocean temperatures, *Tellus, 18*, 820–829, 1966.

Bryan, K., and L. J. Lewis, A water mass model of the world oceans, *J. Geophys. Res., 84*, 2503–2517, 1979.

Bunker, A. F., Computations of surface energy flux and annual air-sea interaction cycles of the North Atlantic Ocean, *Mon. Weather Rev., 104*, 1122–1140, 1976.

Ciesielski, P. E., Variability within the ocean-atmospheric system over the North Pacific, *Environ. Res. Pap., 25*, 97 pp., 1980.

Daly, A. W., The response of North Atlantic sea surface temperature to atmospheric processes, *Q. J. R. Meteorol. Soc., 104*, 363–382, 1978.

Denman, K. L., A time-dependent model of the upper ocean, *J. Phys. Oceanogr., 3*, 173–184, 1973.

Denman, K. L., and M. Miyake, Upper layer modification at Ocean Station 'Papa': Observations and simulation, *J. Phys. Oceanogr., 3*, 185–196, 1973.

De Szoeke, R. A., and P. B. Rhines, Asymptotic regimes in mixed-layer deepening, *J. Mar. Res., 34*, 111–116, 1976.

Elsberry, R. L., and R. W. Garwood, Jr., Numerical ocean prediction models—Goal for the 1980's, *Bull. Am. Meteorol. Soc., 61*, 1556–1566, 1980.

Esbensen, S. K., and R. W. Reynolds, Estimating monthly averaged air-sea transfers of heat and momentum using the bulk aerodynamic method, *J. Phys. Oceanogr., 11*, 457–465, 1981.

Gill, A. E., and J. S. Turner, A comparison of seasonal thermocline models with observation, *Deep Sea Res., 23*, 391–401, 1976.

Halpern, D., Observations of the deepening of the wind-mixed layer in the northeast Pacific Ocean, *J. Phys. Oceanogr., 4*, 454–466, 1974.

Haney, R. L., A numerical case study of the development of large-scale thermal anomalies in the central North Pacific Ocean, *J. Phys. Oceanogr., 16*, 541–556, 1980.

Haney, R. L., W. S. Shiver, and K. H. Hunt, A dynamical-numerical study of the formation and evolution of large-scale ocean anomalies, *J. Phys. Oceanogr., 8*, 952–969, 1978.

Kato, H., and O. M. Phillips, On the penetration of a turbulent layer into a stratified fluid, *J. Fluid Mech., 37*, 643–655, 1969.

Kitaigorodsky, A. N., and Y. Z. Miropolsky, On the theory of open-ocean active layer, *Izv. Akad. Nauk. SSSR Atmos. Ocean. Phys., 6*, 97–102, 1970.

Kondo, J., Y. Sasano, and T. Ishii, On wind-driven current and temperature profiles with diurnal period in the oceanic planetary boundary layer, *J. Phys. Oceanogr., 9*, 360–372, 1979.

Kraus, E. B., and J. S. Turner, A one-dimensional model of the seasonal thermocline, II, The general theory and its consequences, *Tellus, 19*, 98–106, 1967.

Levitus, S., Climatological atlas of the world ocean, *NOAA Prof. Pap., 13*, 173 pp., 1982.

Levitus, S., and A. H. Oort, Global analysis of oceanographic data, *Bull. Am. Meteorol. Soc., 58*, 1270–1284, 1977.

Madsen, O. S., A realistic model of the wind-induced Ekman boundary layer, *J. Phys. Oceanogr., 1*, 248–255, 1977.

Marchuk, I. G., V. P. Kochergin, V. I. Klimok, and V. A. Sukhorukov, On the dynamics of the ocean surface mixed layer, *J. Phys. Oceanogr., 7*, 868–875, 1977.

Mellor, G. L., and P. A. Durbin, The structure and dynamics of the ocean surface mixed layer, *J. Phys. Oceanogr., 5*, 718–728, 1975.

Mellor, G. L., and T. Yamada, A hierarchy of turbulence closure models for planetary boundary layers, *J. Atmos. Sci., 31*, 1791–1806, 1974.

Middleton, J. W., A cross-spectral study of the spatial relationships in the North Pacific sea-surface temperature anomaly field, *Environ. Res. Pap., 23*, 123 pp., 1980.

Miyakoda, K., and A. Rosati, The variation of sea surface temperature in 1976 and 1977, I, The data analysis, *J. Geophys. Res., 87*, 5667–5680, 1982.

Miyakoda, K., and J. Sirutis, Comparative integrations of global models with various parameterized processes of subgrid-scale vertical transports: Description of the parameterization, *Beitr. Phys. Atmos.*, *50*, 445–487, 1977.

Namias, J., and R. M. Born, Temporal coherence in north Pacific sea-surface temperature patterns, *J. Geophys. Res.*, *75*(30), 5952–5955, 1970.

Namias, J., and R. M. Born, Empirical techniques applied to large-scale and long-period air-sea interactions: A preliminary report, *Ref. Ser. 72-1*, Scripps Inst. of Oceanogr., Univ. of Calif., San Diego, 1972.

Namias, J., and R. M. Born, Further studies of temporal coherence in North Pacific sea surface temperature, *J. Geophys. Res.*, *79*, 797–798, 1974.

Niiler, P. P., Deepening of the wind-mixed layer, *J. Mar. Res.*, *33*, 405–422, 1975.

Oort, A. H., The interannual variability of atmospheric circulation statistics, *NOAA Prof. Pap.*, *8*, 76 pp., 1977.

Petterssen, S., *Weather Analysis and Forecasting*, 428 pp., McGraw-Hill, New York, 1956.

Philander, S. G. H., and R. C. Pacanowski, The oceanic response to cross-equatorial winds (with application to coastal upwelling in low latitudes), *Tellus*, *33*, 201–210, 1981.

Pollard, R. T., P. B. Rhines, and R. O. R. Y. Thompson, The deepening of the wind-wind layer, *Geophys. Fluid Dyn.*, *3*, 381–404, 1973.

Ratcliffe, R. A. S., and R. Murray, New lag associations between North Atlantic sea temperature and European pressure applied to long-range weather forecasting, *Q. J. R. Meteorol. Soc.*, *96*, 226–246, 1970.

Reynolds, R. W., A comparison of sea surface temperature climatologies, *J. Clim. Appl. Meteorol.*, *22*, 447–459, 1983.

Richtmyer, R. D., and K. W. Morton, *Difference Methods for Initial-Value Problems*, 2nd ed., 405 pp., Interscience, New York, 1967.

K. Miyakoda and A. Rosati, Geophysical Fluid Dynamics Laboratory/National Oceanic and Atmospheric Administration, Princeton University, Princeton, NJ 08542.

(Received November 15, 1981;
revised March 19, 1984;
accepted March 19, 1984.)